

# Phase Fresnel Lens Development for X-ray & Gamma-ray Astronomy

John Krizmanic<sup>1,2</sup>, Robert Streitmatter<sup>2</sup>, Zaven Arzoumanian<sup>1,3</sup>, Vlad Badilita<sup>4</sup>, Keith Gendreau<sup>3</sup>,  
Neil Gehrels<sup>2</sup>, Reza Ghodssi<sup>4</sup>, Brian Morgan<sup>4,‡</sup>, Gerry Skinner<sup>1,6</sup>

1 CRESST/Universities Space Research Association

2 NASA GSFC, Code 661, Greenbelt, Maryland 20771

3 NASA GSFC, Code 662, Greenbelt, Maryland 20771

4 Dept. of Electrical and Computer Engineering, University of Maryland, College Park, Maryland 20742

6 Dept. of Astronomy, University of Maryland, College Park, Maryland 20742

‡ current address, U.S. Army Research Laboratory, Adelphi, MD 20783

**Abstract- Observations in the hard X-ray and gamma-ray energy regimes are constrained by limited sensitivity and angular resolution. Significant gains could be made if these high-energy photons could be concentrated from a large area onto a small detector element and if diffraction-limited measurements could be obtained. Furthermore, the angular resolution in the gamma-ray band would be superior to that possible at all other wavelengths since the diffraction-limited angular resolution improves with increasing energy. Phase Fresnel Lenses (PFL's) have high throughput at hard x-ray and gamma-ray energies, can achieve, in principle, diffraction-limited angular resolution, and have the capability of being scaled to large dimensions. We have successfully fabricated PFL's and measured near diffraction-limited performance with high efficiency in focusing 8 keV x-rays at the GSFC 600-meter Interferometry Testbed. The results demonstrate the superior imaging potential in the x-ray/gamma-ray energy band for PFL-based optics in a format that is scalable for astronomical applications.**

## I. INTRODUCTION

Astronomical observations in the x-ray and gamma-ray energy regime have been essential in furthering our understanding of astrophysical processes. However, such observations in the x-ray and especially the gamma-ray energy band, have been constrained due to limited sensitivity and poor angular resolution. While Chandra has demonstrated measurements with fraction of an arcsecond imaging at photon energies  $<10$  keV [1], the current angular resolution performance for energies  $> 10$  keV is far poorer. That obtained by the INTEGRAL mission [2], is  $15'$ , nearly the angular radius of the full moon. Balloon-borne instruments, such as InFOCuS [3] and HEFT [4], have exhibited angular resolutions of  $\sim 2'$ , and the planned SIMBOL-X mission [5] is anticipated to obtain an angular resolution of  $\sim 15''$  in this  $>10$  keV energy range. The limitations on imaging astronomical phenomena at these energies are due to the inherent difficulty

in optically concentrating the incident high-energy photons onto an appropriate detector.

Diffraction optics, in particular Phase Fresnel Lenses (PFL's), offer the ability to construct large, diffraction-limited, and highly efficient x-ray/ $\gamma$ -ray optics leading to dramatic improvement in source sensitivity and angular resolution [6,7]. As the diffraction limit improves with increasing photon energy,  $\gamma$ ray photons offer the potential to obtain the best angular resolution over the entire electromagnetic spectrum. A major improvement in source sensitivity can be achieved if a meter-size PFL can be constructed, as the entire area focuses photons.

A meter-size PFL imaging  $\sim 100$  keV photons with a sufficiently large focal length would have an inherent angular resolution measured in micro-arcseconds ( $\mu''$ ). This superb angular resolution is many orders of magnitude improvement compared to what is currently achievable in this energy range. Furthermore, more modest-size PFL's can provide milli-arcsecond ( $m''$ ) imaging in the hard x-ray energy range with relatively short focal lengths.

We have employed Micro-Electro-Mechanical-System (MEMS) fabrication techniques, specifically gray-scale lithography, to fabricate silicon PFL's of substantial diameters in a format scalable for astronomical implementation, with micron minimum feature size and focal length appropriate for ground tests and have characterized their imaging properties. This development has demonstrated that the required tolerances are achievable with the gray-scale fabrication process. Moreover, we have perfected the technique to yield PFL radial profiles close to the ideal, which translates into highly efficient imaging.

## II. PFL's: PRINCIPLE OF OPERATION

A Phase Fresnel Lens (PFL) is a circular diffraction grating with the pitch of the  $N$  concentric annuli becoming smaller in a prescribed manner as the radius of the lens increases. The radial profile of each annulus, or Fresnel zone, in an ideal PFL is *exactly matched* to the optical path needed to coherently concentrate incident radiation into the primary focus [8]. Coherent imaging leads to focused flux gains  $\approx N^2$  where  $N$  is the number of Fresnel zones in the lens. The thickness of material is varied in each Fresnel zone from zero to a maximum thickness of  $t_{2\pi}$ , the length required to obtain a  $2\pi$  phase shift for the material at a specific photon energy.

In an ideal PFL, all power is concentrated into the first order focus and a maximum theoretical efficiency approaching 100% is obtained. This is to be compared to the efficiencies for other diffractive optics that approximate the required lens profile over each Fresnel zone: the theoretical maximum efficiency for a Fresnel Zone Plate is  $\sim 10\%$  while that for a Phase-Reverse Zone Plate is  $\sim 41\%$ . In practice, the exact Fresnel zone profile of a PFL is approximated by a number of steps ( $P$ ), as illustrated in Fig. 1, with the performance improving as the number of steps increases. Choosing the radial step locations to yield equal annular areas yields the maximum efficiency at the primary focus [9].

Ignoring absorption, the efficiency at the primary focus,  $\eta$ , for a  $P$ -stepped PFL profile is [10]

$$\eta = \left[ \frac{\sin(\pi/P)}{(\pi/P)} \right]^2 \quad (1)$$

In the case of an ideal PFL profile,  $P \rightarrow \infty$  and all incident energy is concentrated at the 1<sup>st</sup> order focus yielding a maximum theoretical efficiency of 100%. Equation (1) yields an efficiency of 95% for the case for an 8-stepped PFL as shown in Fig. 1

The index of refraction of a material is expressed as  $n^* = 1 - \delta - i\beta$ . Above  $\sim 30$  eV, the refractive index decrement,  $\delta$ , is small and positive and the imaginary part,  $\beta$ , corresponding to absorption in the material. A thickness  $t$  will attenuate the incident photon flux by  $e^{-t/\tau}$  where  $\tau = (4\pi\beta)^{-1}$  and retard the phase by  $\phi = 2\pi t/\lambda$ . The thickness needed to retard the phase by  $2\pi$  is given by  $t_{2\pi} = \lambda/\delta$  leading to an ideal PFL profile given by  $t(r) = t_{2\pi} \text{MOD}[r^2/(2f\lambda), 1]$  where  $f$  is the focal length,  $r$  the lens radius, and  $\text{MOD}$  is the *modulo* function. Away from absorption edges and apart from small corrections, the thickness needed to provide a  $2\pi$  phase shift in a material,  $t_{2\pi}$ , is an increasing function of energy. The efficiency, at the primary focus, taking into account absorption is expressed as [9]

$$\eta' = \frac{1}{4\pi^2} \left[ \sum_{i=1}^P e^{-t_i/2\tau} \int_{\psi_{i-1}}^{\psi_i} e^{i(\theta - \varphi_i)} d\theta \right]^2 \quad (2)$$

where  $I_0$  is the incident irradiance and  $t_i$  is the thickness of the  $i^{\text{th}}$  step that induces a phase retardation  $\varphi_i$ . The locations of the  $i^{\text{th}}$  step transitions, in terms of their relative phase in a particular Fresnel zone, are given by  $\psi_{i-1}$  and  $\psi_i$ . The

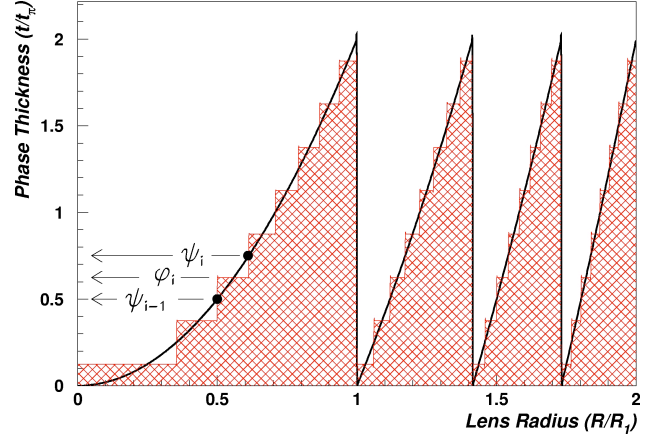


Fig. 1. Octonary-stepped ( $P=8$ ) PFL profile for the first 4 Fresnel zones. The curve shows the ideal PFL profile. The lens radius is given in terms of  $R_1 (= \sqrt{2f\lambda})$ , the radius of the first Fresnel zone.

implementation of (2) is straightforward and allows for the determination of the design efficiency for a PFL including the effects of absorption.

The focal length ( $f$ ) of a PFL is related to the smallest pitch of the Fresnel pattern ( $P_{Min}$ , located on the outermost lens radii), the diameter of the lens ( $d$ ), and the photon energy ( $E_\gamma$ ), and is given by

$$f = P_{Min} d / 2\lambda = 4 \times 10^2 \left[ \frac{P_{Min}}{1 \text{ mm}} \right] \left[ \frac{d}{1 \text{ m}} \right] \left[ \frac{E_\gamma}{1 \text{ keV}} \right] \text{ km} \quad (3)$$

which implies long focal lengths are required for the construction of a large optic for an astronomical instrument to fully realize the gain in angular resolution offered by this technique. This necessitates placement of the lens and the photon detector on separate spacecraft in a formation-flying configuration.

### III. GROUND-TEST PFL FABRICATION

While diffractive optics have been employed in x-ray microscopy, e.g. [11], these devices have small diameters of 1 mm or less, a minimum Fresnel zone pitch measured in nanometers, and operate at short focal lengths of the order of a meter since imaging a low photon flux is not a dominant issue but spatial resolution is important. In an astronomical implementation, the requirement to image the small photon flux detected at Earth emitted from distant astrophysical objects drives the diameter of the PFL to be maximized. The construction of a large diameter PFL with minimum Fresnel zone pitch in the micron range is practical and is in the realm of MEMS fabrication techniques.

We have employed the gray-scale lithographic technique to fabricate silicon PFL's of substantial diameters in a format scalable for astronomical implementation [12], with micron minimum feature size and focal length appropriate for ground tests and have characterized their imaging properties. The gray-scale mask design and lithography were performed

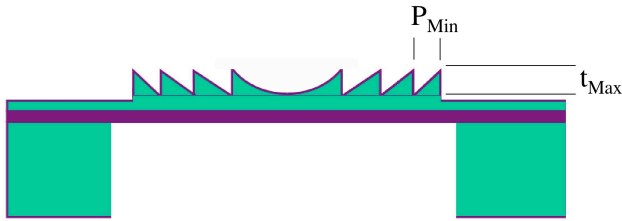


Fig. 2. Schematic of the membrane suspended PFL structure on an SOI wafer after DRIE removal of the substrate to decrease absorption.

at the University of Maryland, and a description of this technique follows. An optical mask is generated with the desired structure built from small, varying opacity pixels. By modulating the intensity of light through a gray-scale optical mask, a positive photoresist that was spun onto a silicon substrate is partially exposed to different depths. After development, a 3-dimensional profile made of ‘gray levels’ will remain in the photoresist corresponding to the intensity pattern generated on the optical mask. The structure is then transferred into the silicon via an anisotropic, Deep-Reactive-Ion-Etch (DRIE) to fabricate the desired device.

The fabricated PFL’s were designed to image at 8 keV ( $\text{Cu K}\alpha$ ) with a focal length of 112.5 meters and tested in the NASA GSFC 600-meter X-ray Interferometry Testbed. Fabricated on top of a  $30\ \mu\text{m}$  thick substrate, these PFL’s had thickness of  $t_{Max} = 2 \times t_{2\pi} \approx 40\ \mu\text{m}$  with a Fresnel ridge pitch spanning 2 full Fresnel zones. This effectively doubles the minimum Fresnel ridge spacing (at the outermost radii) at the expense of accepting a modest reduction in efficiency. More practically, this doubles the diameter of a PFL for a given minimum Fresnel ridge spacing ( $P_{Min}$ ) but with no change to the required aspect ratio, i.e.  $t_{Max}/P_{Min}$ .

Table 1 details the design parameters of four different fabricated PFL’s designed for 8 keV imaging with a focal length of 112.5 meters. These four lenses along with associated test structures were fabricated on the same gray-

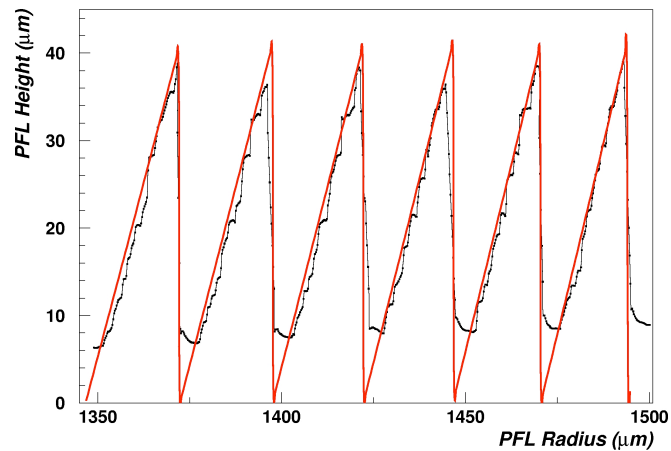
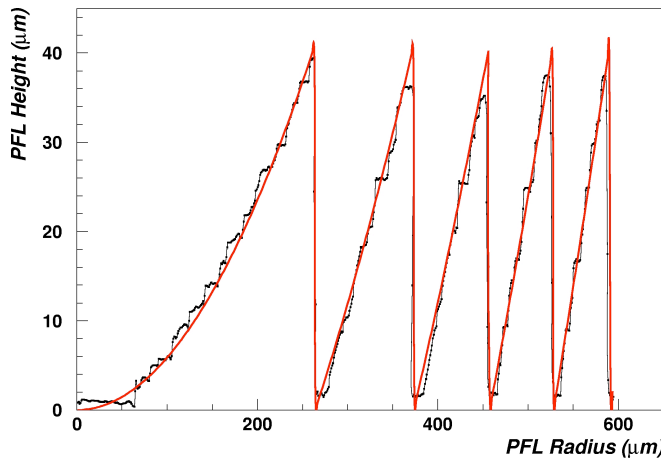


Fig. 4. The measured profiles of the 3 mm diameter PFL characterized in the 600 meter test beam. The left plot shows the measurement of the Fresnel profile at the center of the PFL while the right plot shows that for the profile near the outermost radii. The continuous curves represent the ideal profile.

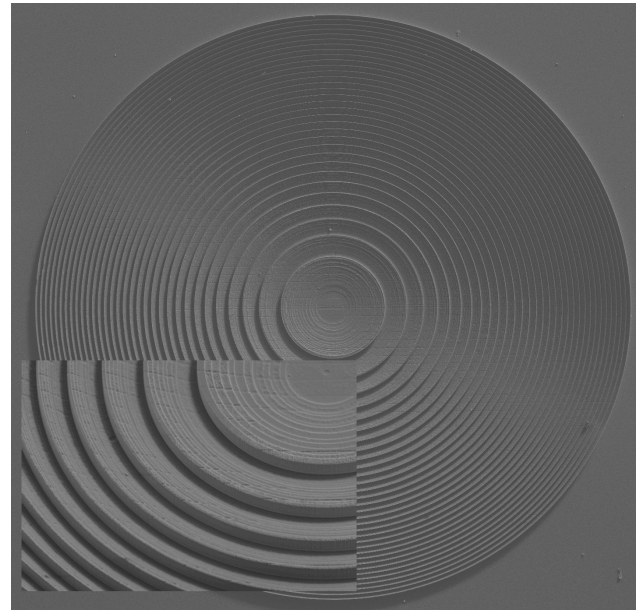


Fig. 3. A SEM of the 3 mm PFL tested at 8 keV. The inset shows a zoom of the inner part of the Fresnel profile.

scale optical mask, and a step-and-repeat process filled a 100 mm silicon wafer with an array of PFL’s. In order to minimize absorption, the PFL’s were fabricated using Silicon-On-Insulator (SOI) wafers that allowed for the removal of silicon under each PFL to leave a  $30\ \mu\text{m}$  membrane under each PFL. A ‘hole’ was etched through the  $500\ \mu\text{m}$  thick silicon substrate using DRIE after double-side alignment with the  $40\ \mu\text{m}$  tall PFL structure on top. The  $2\ \mu\text{m}$  buried oxide is a natural etch stop in the DRIE etch of silicon. Thus the PFL is suspended on a thin membrane with the wafer maintaining the necessary mechanical rigidity. A schematic of the SOI implementation is shown in Fig. 2, and a SEM of a beam-tested PFL is shown in Fig. 3.

Table I

Design Parameters for the fabricated PFL's. Levels/ $4\pi$  Ridge represents the number of steps approximating the ideal PFL profile while the # Ridges are the total number of Fresnel annuli for each PFL. Note two of the PFL's are identical.

PFL Diameter	$P_{Min}$	Levels/ $4\pi$ Ridge	# Ridges
3 mm	24 $\mu\text{m}$	16	32
3 mm	24 $\mu\text{m}$	16	32
3 mm	24 $\mu\text{m}$	8	32
4.72 mm	15 $\mu\text{m}$	8	80

After fabrication, the individual PFL's were visually inspected and were characterized via optical profilometer measurements. These results were used with a variation of (2) to obtain an estimate of the anticipated efficiency for each lens. Several PFL's that exhibited high, anticipated efficiencies were selected for incorporation in the x-ray beam tests. Fig. 3 shows the measured profiles at the center and outer radii of a beam-tested, 3 mm PFL along with a comparison to the ideal profile.

#### IV. BEAM TEST RESULTS

The characterization of the imaging properties of the PFL's was performed at the NASA GSFC 600-meter X-ray Interferometry Testbed. The PFL under test was placed approximately 150 meters from a copper-target, micro-focus x-ray source and a LN<sub>2</sub>-cooled CCD x-ray camera located approximately 450 meters downstream from the PFL. The CCD contained 1024x1024, 13x13  $\mu\text{m}^2$  pixels and demonstrated an energy resolution of 150 eV (FWHM) at 8 keV (Cu K $\alpha$ ). The beam line and chamber containing the PFL's was held at a < 100 mTorr pressure during testing. Fig. 5 shows the 'first light' results of a PFL imaging 8 keV x-rays.

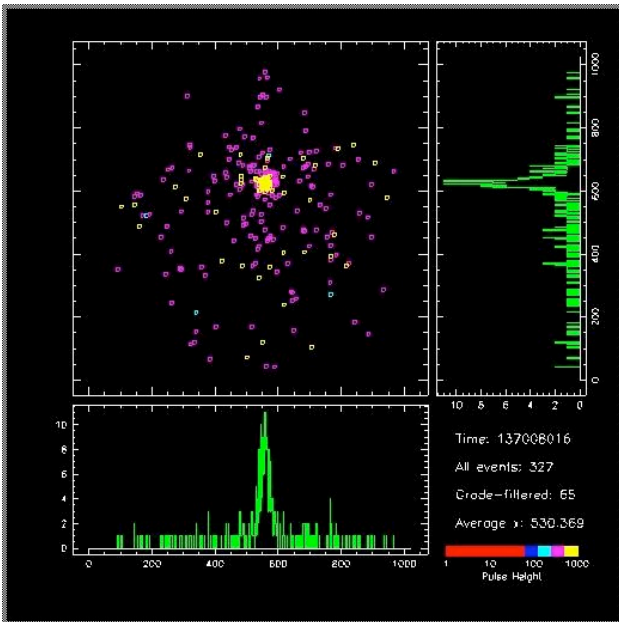


Fig. 5. The 'first light' results showing 8 keV x-rays imaged by a PFL.

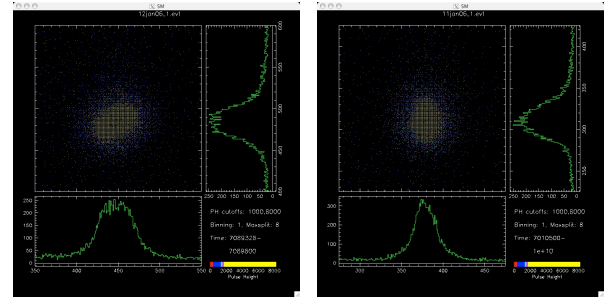


Fig. 6. The  $40 \times 60 \mu\text{m}^2$  elliptical spot of the x-ray source as imaged by a PFL. The source was mechanically rotated by 60 degrees between the two exposures. The images span  $200 \times 200$  CCD pixels (each  $13 \times 13 \mu\text{m}^2$ ).

Fig. 6 shows the image of the elliptical  $40 \times 60 \mu\text{m}^2$  x-ray spot of the source as imaged by a 3 mm diameter PFL and measured by the CCD x-ray camera. The size of the x-ray spot was confirmed by pinhole scans and the elliptical geometry verified by rotating the x-ray tube and thus the orientation of the imaged spot. The ability to discern  $20 \mu\text{m}$  over 150 m yields an angular resolution of  $28 \text{ m}''$ , which is a approximately a factor of two away from the diffraction limit of  $13 \text{ m}''$ .

Using calibration measurements, the efficiency was determined to be 35% at 8 keV, compared to the theoretical maximum of 50%, obtained using (2), and includes the absorptive effects of the PFL and  $30 \mu\text{m}$  substrate. The reduction in the measured efficiency as compared to the theoretical maximum is caused by the fabricated PFL profile being away from the ideal, as illustrated in Fig. 3. Another effect is apparent: a gradual thickening of the substrate as the radius of the PFL increases. This substrate thickening is caused by an aspect-ratio dependence in the fabrication, i.e. it is more difficult to remove silicon between ridges as the Fresnel ridge spacing becomes narrower at the outermost radii. Further development of the gray-scale process has demonstrated that the aspect-ratio dependence can be compensated in the design, and leads to a uniform substrate thickness [13].

#### V. SECOND GENERATION PFL'S

This Compensated Aspect Ratio Dependent Etch (CARDE) technique has been employed in the fabrication of a second-generation PFL's designed to image at the 17.4 keV (Mo K $\alpha$ ). The gray-scale process has also been refined such that the achievable minimum Fresnel ridge pitch,  $P_{Min}$ , has been reduced to  $5 \mu\text{m}$ . As implied by (3), this along with the required increase in aspect-ratio in the DRIE process has allowed the fabrication of second-generation, 3 mm PFL's designed to image 17.4 keV photons with a focal length of approximately 112 meters. This fabrication capability is demonstrated in Fig. 7, showing a SEM of a Fresnel test structure, with  $10 \mu\text{m}$  ridge spacing.

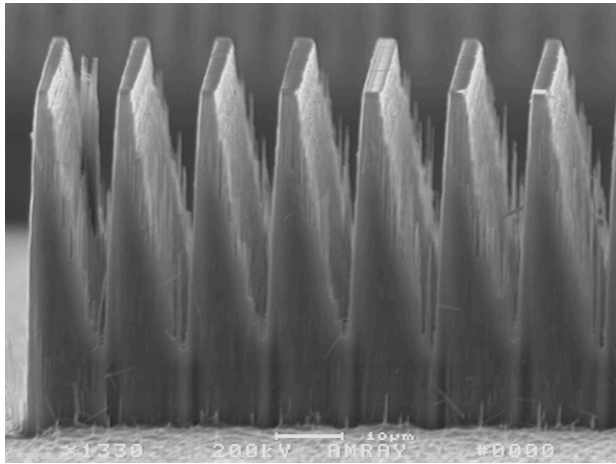


Fig. 7. A Fresnel test structure with 10  $\mu\text{m}$  ridge spacing and 90  $\mu\text{m}$  height.

## VI. CONCLUSION

We have fabricated silicon PFL's, using the gray-scale lithographic technique, in a scalable format suitable for astronomical instrumentation. We have characterized the imaging properties of these PFL's in a 600 meter x-ray beam line. The results demonstrate near diffraction-limited imaging with high collection efficiency at 8 keV. This development has demonstrated that the required tolerances are achievable with the gray-scale fabrication process. Moreover, we have perfected the technique to yield PFL radial profiles close to the ideal, which translates into highly efficient imaging. This has led to the fabrication of second-generation PFL's, of substantial size, designed to image at a higher, 17.4 keV x-ray energy.

This research is supported under NASA NNH04ZSS001N-APRA.

## REFERENCES

- [1] M.C. Weisskopf et al., ,Pub. Astron. Soc. Pac. 114, 1 (2002)
- [2] C. Winkler et al., "The INTEGRAL mission", Astron. & Astrophys. 411, L1 (2003)
- [3] J. Tueller et al., "Infocus hard X-ray imaging telescope," Exp. Astron. 20, 121 (2005)
- [4] F.A. Harrison et al., "Development of the *HEFT* and *NuStar* focusing telescopes," Exp. Astron. 20, 131 (2005)
- [5] G. Pareschi and P. Ferrando, "The SIMBOL-X hard X-ray mission," Exp. Astron. 20, 139 (2005)
- [6] G. Skinner, "Diffractive/refractive optics for high energy astronomy. I. Gamma-ray phase Fresnel lenses," Astron. Astrophys. 375, 691 (2001)
- [7] G. Skinner, "Diffractive-refractive optics for high energy astronomy. II. Variations on the theme," Astron. Astrophys. 383, 352 (2002)
- [8] K. Miyamoto, "The Phase Fresnel Lens", Jour. Opt. Soc. Amer. 51, 17 (1961)
- [9] J. Kirz, "Phase Zone Plates for x rays and the extreme uv", Jour. Opt. Soc. Amer. 64, 301 (1974)
- [10] H. Dammann, "Blazed Synthetic Phase-Only Holograms", Optik 31, 95 (1970)
- [11] E. Di Fabrizio et al., "High-efficiency multilevel zone plates for keV X-rays", Nature, 401, 895 (1999)
- [12] B. Morgan, C.M. Waits, J. Krizmanic, and R. Ghodssi, "Development of a Deep Silicon Phase Fresnel Lens using Gray-scale Technology and

Deep Reactive Ion Etching," Jour. Micro-Electro-Mechanical-Systems (JMEMS), 13, 113 (2004)

- [13] B. Morgan, C.M. Waits, and R. Ghodssi, "Compensated aspect ratio dependent etching (CARDE) using gray-scale technology", Microelectronic Engineering 77, 85 (2005)